

A robust S_N -DG-approximation for radiation transport in optically thick and diffusive regimes

J.C. Ragusa^{a,*}, J.-L. Guermond^{b,1,2}, G. Kanschat^{b,1,2}

^a Department of Nuclear Engineering, Texas A&M University, 3133 TAMU, College Station, TX 77843-3133, United States

^b Department of Mathematics, Texas A&M University, 3368 TAMU, College Station, TX 77843-3368, United States

ARTICLE INFO

Article history:

Received 20 October 2010

Received in revised form 21 October 2011

Accepted 10 November 2011

Available online 22 November 2011

Keywords:

Discontinuous Galerkin

Radiation transport

Thick diffusion limit

Upwind technique

ABSTRACT

We introduce a new discontinuous Galerkin (DG) method with reduced upwind stabilization for the linear Boltzmann equation applied to particle transport. The asymptotic analysis demonstrates that the new formulation does not suffer from the limitations of standard upwind methods in the thick diffusive regime; in particular, the new method yields the correct diffusion limit for any approximation order, including piecewise constant discontinuous finite elements. Numerical tests on well-established benchmark problems demonstrate the superiority of the new method. The improvement is particularly significant when employing piecewise constant DG approximation for which standard upwinding is known to perform poorly in the thick diffusion limit.

© 2011 Elsevier Inc. All rights reserved.

1. Introduction

Spatial discontinuous Galerkin (DG) finite element techniques applied to discrete-ordinates radiation transport have been pioneered by Reed and Hill [16] and Lesaint and Raviart [14] in the early 1970s. They use an upwinding procedure to link mesh cells in order to adequately propagate the flow of information from upwind to downwind cells. Upwinding is viewed as a stabilization technique in the numerical analysis community. Upon adopting this point of view, we redefine the stabilization term and show that the resulting new DG method behaves properly in the thick diffusion limit. Optically thick and diffusive regimes occur when the physical medium is many mean free paths thick and the interaction processes are scattering-dominated (i.e., weak absorption). In the present paper we adopt the terminology of Babuška and Suri [3] “a numerical scheme for the approximation of a parameter-dependent problem is said to exhibit locking if the accuracy of the approximations deteriorates as the parameter tends to a limiting value. A robust numerical scheme for the problem is one that is essentially uniformly convergent for all values of the parameter.” Larsen pointed out in [10,11] that the so-called “step scheme”, a finite volume scheme (i.e., a piecewise constant DG scheme) with standard upwind, locks in the diffusion limit. A modification of the “step scheme” depending upon the total mean free path was proposed in [10] to correct the locking of the method in the diffusion limit, but this required modifying the streaming term and abandoning particle balance. Several other variations of the “step scheme” have been analyzed in [12]: it was shown that the “Lund–Wilson” and the “Castor” variants of the step scheme yielded cell-edge angular fluxes that lock in the diffusion limit, and that the auxiliary relations linking the outgoing edge angular flux to the cell-average angular flux employ a multiplicative factor that depends on the mesh cell optical thickness in the direction traveled. Furthermore, the cell-edge fluxes for these schemes can not reproduce the infinite medium

* Corresponding author.

E-mail addresses: ragusa@ne.tamu.edu (J.C. Ragusa), guermond@math.tamu.edu (J.-L. Guermond), kanschat@tamu.edu (G. Kanschat).

¹ Supported in part by the Department of Homeland Security under Grant No. 2009-DN-077-ARI018-03.

² Supported in part by the National Science Foundation under Grant No. DMS-0713829.

solution. A “new” scheme was proposed in [12] but was subsequently dismissed due its a poor behavior at the boundaries. For many years, the diamond-difference scheme was found to be the best performing finite-difference scheme, even though its cell-edge fluxes lock in the thick diffusion limit. In [13], most of the previous schemes have been set aside in favor of the linear discontinuous finite element scheme (the piecewise linear DG technique with standard upwinding).

In [1], Adams analyzed multi-dimensional DG approximations and showed that some schemes lock in the diffusion limit because the upwind method forces the scalar flux, and thus the angular flux, to be continuous across mesh cells. This observation has been confirmed in [8], where the equivalence of the limit problem to a mixed discretization for the Laplacian was proved and the nature of the boundary layers was discussed. The asymptotic analysis in [1,8] suggests that the problem could be alleviated by modifying the upwind numerical flux. As pointed out in [2,7], the upwind numerical flux is only one particular choice among many for stabilization. By making the amount of stabilization dependent on the scattering cross section so that the amount of upwinding decreases as the scattering cross section increases, we show in this paper that locking can indeed be avoided in the thick diffusive limit. The proposed DG scheme converges robustly, i.e., it performs well in all regimes, from transport-dominated to diffusion-dominated, for finite element spaces of any order, including piecewise constant functions (DG0).

The paper is organized as follows. Section 2 introduces notation and recalls the S_N transport equation. Section 3 describes the discrete formulation which is obtained when applying a discontinuous Galerkin technique to the S_N equations. A new DG numerical flux is introduced therein. The asymptotic analysis of the resulting discrete formulation is done in Section 4. The main result of this section is the demonstration that, in the diffusion limit, the new DG method is a consistent and convergent DG discretization of the diffusion equation written in mixed form. Numerical results illustrating the performance of the new DG numerical flux are presented in Section 5. An Appendix detailing the asymptotic analysis in one space dimension for DG0 completes the paper.

2. The S_N transport equation

2.1. The continuous problem

The linear transport equation describes the processes by which particles (photons, neutrons, ...) interact with a background medium. Such processes play a crucial role in stellar atmospheres, nuclear reactor analysis, and shielding applications. To keep the discussion simple, we limit the analysis to the one-group discrete-ordinates equations; these equations model one-group neutron transport and grey radiative transfer.

Before recalling the transport equation, we provide some notations for the spatial and angular domains. Let \mathcal{D} be the spatial domain in \mathbb{R}^d (with $d = 1, 2, 3$), $\partial\mathcal{D}$ be the boundary of \mathcal{D} , \mathbf{n} be the outward unit normal vector on $\partial\mathcal{D}$, and S^2 be the unit sphere in \mathbb{R}^3 . The set of directions \mathcal{S} is defined as S^2 for $d = 3$ and as the projection of S^2 onto \mathbb{R}^d when $d = 1, 2$. For instance \mathcal{S} is the unit disk if $d = 2$ and \mathcal{S} is the unit segment $[-1, +1]$ if $d = 1$. This is a common practice in the radiation transport community and it means that radiation is accounted for as a three-dimensional effect even in lower dimensional geometries. The transport of particles is modeled by the linear Boltzmann equation:

$$\boldsymbol{\Omega} \cdot \nabla \Psi(\boldsymbol{\Omega}, \mathbf{x}) + \sigma_t(\mathbf{x})\Psi(\boldsymbol{\Omega}, \mathbf{x}) - \sigma_s(\mathbf{x})\bar{\Psi}(\mathbf{x}) = q(\mathbf{x}), \quad \forall (\boldsymbol{\Omega}, \mathbf{x}) \in \mathcal{S} \times \mathcal{D}, \tag{1a}$$

where $\bar{\Psi} = \frac{1}{4\pi} \int_{\mathcal{S}} \Psi(\boldsymbol{\Omega}, \mathbf{x}) d\boldsymbol{\Omega}$ is the the scalar flux, and the boundary conditions are

$$\Psi(\boldsymbol{\Omega}, \mathbf{x}) = \Psi^{\text{inc}}(\boldsymbol{\Omega}, \mathbf{x}), \quad \forall (\boldsymbol{\Omega}, \mathbf{x}) \in \mathcal{S} \times \partial\mathcal{D}, \quad \boldsymbol{\Omega} \cdot \mathbf{n}(\mathbf{x}) < 0. \tag{1b}$$

For simplicity, we have assumed that the scattering and the extraneous sources are isotropic; this assumption does not affect the conclusions of the analysis. The dependent variable is the angular flux $\Psi(\boldsymbol{\Omega}, \mathbf{x})$, and the independent variables $(\boldsymbol{\Omega}, \mathbf{x})$ span $\mathcal{S} \times \mathcal{D}$. The given data are the extraneous source term $q(\mathbf{x})$, the incoming boundary radiation $\Psi^{\text{inc}}(\boldsymbol{\Omega}, \mathbf{x})$, the scattering cross section $\sigma_s(\mathbf{x})$, and the absorption cross section $\sigma_a(\mathbf{x})$ (with the usual definition $\sigma_t = \sigma_s + \sigma_a$).

2.2. The S_N problem

The S_N , or discrete-ordinates, version of Eq. (1a) is obtained by solving the transport equation along discrete directions (or ordinates) and by replacing the integrals over the unit sphere \mathcal{S} by quadratures. We choose a quadrature rule $\{(\boldsymbol{\Omega}_j, \omega_j), j = 1, \dots, n_\Omega\}$ with the normalization

$$\sum_j \omega_j = 1, \quad \text{so that} \quad \frac{1}{4\pi} \int_{\mathcal{S}} f(\boldsymbol{\Omega}, \mathbf{x}) d\boldsymbol{\Omega} \approx \sum_{j=1}^{n_\Omega} \omega_j f(\boldsymbol{\Omega}_j, \mathbf{x}). \tag{2}$$

Next, we recall some quadrature properties that will be employed later, during the asymptotic analysis:

- (i) Symmetry: For any discrete ordinate $\boldsymbol{\Omega}_j$ in the quadrature set, its opposite $\boldsymbol{\Omega}_j = -\boldsymbol{\Omega}_j$ is also in the set and their weights are equal ($\omega_j = \omega_j$). This implies in particular that

$$\sum_{j=1}^{n_\Omega} \omega_j \mathbf{\Omega}_j = \mathbf{0}. \tag{3}$$

(ii) For any two vectors \mathbf{a} and \mathbf{b} in \mathbb{R}^d , the angular quadrature satisfies

$$\sum_{j=1}^{n_\Omega} \omega_j (\mathbf{\Omega}_j \cdot \mathbf{a})(\mathbf{\Omega}_j \cdot \mathbf{b}) = \frac{1}{3} \mathbf{a} \cdot \mathbf{b}. \tag{4}$$

(iii) There is $c_0 > 0$ so that the following holds for all n_Ω

$$0 < c_0 \leq c_n := \sum_{\mathbf{\Omega}_j \cdot \mathbf{n} < 0} \omega_j |\mathbf{\Omega}_j \cdot \mathbf{n}|. \tag{5}$$

Although it is a standard result that for any unit vector \mathbf{n} , the half-range integral satisfies $\frac{1}{4\pi} \int_{\mathbf{\Omega} \cdot \mathbf{n} < 0} |\mathbf{\Omega} \cdot \mathbf{n}| d\mathbf{\Omega} = \frac{1}{4}$, this equality may not exactly hold for any numerical quadrature at hand. However, reasonable sets of quadrature rules are such that this limit value is approached as the number of directions in the quadrature is increased ($\lim_{n_\Omega \rightarrow \infty} c_n = \frac{1}{4}$).

The S_N method consists of replacing the angular flux $\Psi(\mathbf{\Omega}, \mathbf{x})$ by a discrete angular flux $\psi(\mathbf{x}) = (\psi_1(\mathbf{x}), \psi_2(\mathbf{x}), \dots, \psi_{n_\Omega}(\mathbf{x}))$, and to convert the integro-differential Eq. (1) over $S \times \mathcal{D}$ into a system of n_Ω coupled partial differential equations over \mathcal{D} , which reads as follows for all directions j :

$$\mathbf{\Omega}_j \cdot \nabla \psi_j(\mathbf{x}) + \sigma_t(\mathbf{x}) \psi_j(\mathbf{x}) - \sigma_s(\mathbf{x}) \bar{\psi}(\mathbf{x}) = q(\mathbf{x}), \quad \text{in } \mathcal{D}, \tag{6a}$$

with the inflow boundary condition

$$\psi_j(\mathbf{x}) = \psi_j^{\text{inc}}(\mathbf{x}), \quad \forall \mathbf{x} \in \partial \mathcal{D} \text{ with } \mathbf{\Omega}_j \cdot \mathbf{n}(\mathbf{x}) < 0. \tag{6b}$$

The discrete scalar flux is defined by:

$$\bar{\psi}(\mathbf{x}) = \sum_{j=1}^{n_\Omega} \omega_j \psi_j(\mathbf{x}). \tag{7}$$

The discrete angular flux ψ is said to be isotropic when $\psi_j = \bar{\psi}$, for all $j \in [1, n_\Omega]$. In order to simplify the notation in subsequent parts, we introduce the discrete current vector $\mathbf{J}(\psi)$, also known as the first angular moment of ψ , as follows:

$$\mathbf{J}(\psi) = \sum_{j=1}^{n_\Omega} \omega_j \psi_j(\mathbf{x}) \mathbf{\Omega}_j. \tag{8}$$

Note that $\mathbf{J}(\psi) = \mathbf{0}$ whenever ψ is isotropic.

3. DG Discretization

We now proceed with the spatial discretization of the S_N transport equation using DG finite elements. We introduce a discrete mesh on \mathcal{D} in Section 3.1, the polynomial spaces and DG notation in Section 3.2, and the weak formulation in Section 3.3. In Section 3.2, we also generalize the definition for upwind and downwind values at cell interfaces.

3.1. The mesh

A mesh \mathbb{T}_h is a subdivision of \mathcal{D} into disjoint cells K (the h subscript is common in the finite element literature and denotes the typical mesh size of the mesh). The mesh can be unstructured since the method is independent of the space dimension and the choice of grid. We denote by \mathbb{F}_h^i the set of *interior* faces (also called interfaces); each face $F \in \mathbb{F}_h^i$ is the intersection of the boundaries of two mesh cells. For each face $F \in \mathbb{F}_h^i$ we assign a normal vector \mathbf{n} . While the choice of the normal vector is arbitrary for interior faces, all formulations below are independent of this choice and thus well-defined. We denote by \mathbb{F}_h^b the set of faces on the domain boundary, $\partial \mathcal{D}$ for which we denote by \mathbf{n} the outward unit normal vector. Finally, we gather all faces into $\mathbb{F}_h = \mathbb{F}_h^i \cup \mathbb{F}_h^b$.

3.2. The discontinuous Galerkin (DG) setting

We define the approximation spaces based on the mesh \mathbb{T}_h , such that functions are polynomials of degree at most k on each mesh cell; the maximum degree k can be chosen arbitrarily and determines the order of the method. In particular, piecewise constant approximation (DGO) is permitted. This already defines the space V_h for the scalar flux, since we do not require any continuity between cells. The discrete space for the angular flux, W_h , simply consists of copies of V_h for each of the discrete ordinates:

$$V_h = \left\{ v \in L^2(\mathcal{D}) \mid \forall K \in \mathbb{T}_h, v|_K \in P_K \right\}, \quad W_h = (V_h)^{n_\Omega}. \tag{9}$$

The set of functions over each cell $K \in T_h$ that can be mapped to polynomials of degree at most k over the reference element is denoted P_K . We also introduce the spaces with zero boundary conditions

$$V_{0,h} = \{ v \in V_h \mid v|_{\partial\mathcal{D}} = 0 \}, \quad W_{0,h} = (V_{0,h})^{n_\Omega}. \tag{10}$$

The purpose of these spaces is for notational conciseness in the asymptotic derivation. Due to the discontinuous nature of the spatial approximation, functions $v \in V_h$ are double-valued on interior faces. Consider an interior face $F \in \mathbb{F}_h^i$ separating two mesh cells, K_1 and K_2 . Denote by $\mathbf{n}_1, \mathbf{n}_2$ the unit normal vector on F pointing towards K_2, K_1 , respectively. The mean value and jump of a function $v \in V_h$ are defined as follows:

$$\{\{v\}\} = \frac{1}{2}(v_1 + v_2), \quad \llbracket v \rrbracket = v_1 - v_2, \tag{11}$$

where $v_1 := v|_{K_1}$ and $v_2 := v|_{K_2}$ are the restrictions of v on the mesh cells K_1 and K_2 , respectively. Obviously, $\{\{v\}\}$ does not depend on the choice (numbering) of the cells K_1 and K_2 . On the other hand, the jump does (there is a sign change when exchanging the cells K_1 and K_2) but since the weak form (defined further below) contains the product of two jumps, the orientation of the unit normal vector does not matter. Note that the mean value of quantities containing a normal vector is actually a jump:

$$\{\{\mathbf{n}\}\} = \frac{1}{2}(v_1 \mathbf{n}_1 + v_2 \mathbf{n}_2) = \frac{1}{2}(v_1 - v_2) \mathbf{n}_1 = \frac{1}{2}(v_2 - v_1) \mathbf{n}_2.$$

The jump and mean value can be used to rewrite the standard upwind numerical flux³ [14,16] found in DG methods approximating the transport equation. For any v in V_h and any interior face $F \in \mathbb{F}_h^i$, we introduce the so-called upwind and downwind values of v at $\mathbf{x} \in F$, $v^+(\mathbf{x})$ and $v^-(\mathbf{x})$, respectively, as follows:

$$v^+(\mathbf{x}) = \begin{cases} v_1(\mathbf{x}), & \text{if } \boldsymbol{\Omega} \cdot \mathbf{n}_1(\mathbf{x}) \geq 0 \\ v_2(\mathbf{x}), & \text{if } \boldsymbol{\Omega} \cdot \mathbf{n}_1(\mathbf{x}) < 0. \end{cases} \quad v^-(\mathbf{x}) = \begin{cases} v_2(\mathbf{x}) & \text{if } \boldsymbol{\Omega} \cdot \mathbf{n}_1(\mathbf{x}) \geq 0 \\ v_1(\mathbf{x}) & \text{if } \boldsymbol{\Omega} \cdot \mathbf{n}_1(\mathbf{x}) < 0. \end{cases} \tag{12}$$

Observing that, for any positive number ($\gamma \geq 0$), we have

$$\boldsymbol{\Omega} \cdot \mathbf{n}_1 \{\{v\}\} + \frac{1}{2} \gamma |\boldsymbol{\Omega} \cdot \mathbf{n}_1| \llbracket v \rrbracket = \boldsymbol{\Omega} \cdot \mathbf{n}_1 \left(v^+(\mathbf{x}) + \frac{1}{2} (\gamma - 1) (v^+(\mathbf{x}) - v^-(\mathbf{x})) \right), \tag{13}$$

we note that the left-hand-side of Eq. (13) reduces to two particular cases when $\gamma = 1$ and $\gamma = 0$:

$$\boldsymbol{\Omega} \cdot \mathbf{n}_1 \{\{v\}\} + \frac{\gamma}{2} |\boldsymbol{\Omega} \cdot \mathbf{n}_1| \llbracket v \rrbracket = \begin{cases} \boldsymbol{\Omega} \cdot \mathbf{n}_1 v^+(\mathbf{x}) & \text{if } \gamma = 1, \\ \boldsymbol{\Omega} \cdot \mathbf{n}_1 \{\{v\}\} & \text{if } \gamma = 0. \end{cases} \tag{14}$$

That is, the standard upwind DG numerical flux on a face is obtained with the expression of Eq. (13) by using $\gamma = 1$ and the centered numerical flux is obtained by using $\gamma = 0$. Thus, the above representation introduces a way to construct an approximation of the solution to Eq. (6) by modifying the coefficient γ . Reduced upwinding has been discussed and applied successfully in the context of advection–diffusion problems in [2,4].

3.3. The new DG formulation

Now we propose a new formulation for the DG numerical flux based on Eq. (13). For this purpose we define the stabilization parameters

$$\gamma(\mathbf{x}) = \frac{\gamma_0}{\max(\gamma_0, \sigma_s(\mathbf{x}) \text{diam}\mathcal{D})}, \quad \delta(\mathbf{x}) = \delta_0 \frac{1 - \gamma(\mathbf{x})}{\gamma(\mathbf{x})}, \tag{15}$$

with coefficients $\gamma_0 > 0, \delta_0 > 0$. The rationale for these is as follows: in the thick diffusive limit, γ tends to 0, whereas in the thin diffusive limit, γ is 1.

Consider an interior face $F \in \mathbb{F}_h^i$. We use the following definition for the angular DG numerical flux across the interface F from K_1 to K_2 :

$$\widehat{\mathbf{F}}_j(\mathbf{x}) \cdot \mathbf{n}_1 = \boldsymbol{\Omega}_j \cdot \mathbf{n}_1 \{\{\psi_j\}\} + \frac{\gamma(\mathbf{x})}{2} |\boldsymbol{\Omega}_j \cdot \mathbf{n}_1| \llbracket \psi_j \rrbracket + \frac{\delta(\mathbf{x})}{2} \{ \{\mathbf{J}(\psi) \cdot \mathbf{n}\} \} \boldsymbol{\Omega}_j \cdot \mathbf{n}_1. \tag{16}$$

³ The term “flux” is used in two different contexts. In the radiation transport context, we use the terms “angular flux” and “scalar flux”. In the DG context, we use the notion of “numerical flux”. These two notions are unfortunately unrelated but commonly employed in the radiation transport and DG literature, respectively. To avoid confusion, we always use the proper adjective in this paper.

The purpose of the numerical flux $\widehat{\mathbf{F}}_j(\mathbf{x}) \cdot \mathbf{n}$ is to approximate the quantity $\mathbf{\Omega}_j \cdot \mathbf{n} \psi_j$ at the mesh interfaces since this quantity is double-valued due to the discontinuous nature of the approximation. For any boundary face $F \in F_h^b$, we use the standard upwind definition of the DG numerical flux across F :

$$\widehat{\mathbf{F}}_j(\mathbf{x}) \cdot \mathbf{n} = \begin{cases} \mathbf{\Omega}_j \cdot \mathbf{n} \psi_j^{\text{inc}} & \text{if } \mathbf{\Omega}_j \cdot \mathbf{n}(\mathbf{x}) < 0, \\ \mathbf{\Omega}_j \cdot \mathbf{n} \psi_j & \text{otherwise.} \end{cases} \tag{17}$$

Note that the definition of $\gamma(\mathbf{x})$ is such that, on the one hand, $\gamma \rightarrow 0$ when the ratio of the scattering mean free path to the diameter of the domain is small (i.e., $\sigma_s(\mathbf{x})\mathcal{D}$ is large); on the other hand, γ is bounded away from zero when the mean free path is a non-negligible fraction of the diameter of the domain (the γ_0 constant assures that $\gamma(\mathbf{x}) \rightarrow 1$ when $\sigma_s(\mathbf{x})\mathcal{D}$ is small). The parameter δ is designed so that it goes to zero when $\gamma \rightarrow 1$ and behaves like $1/\gamma$ when $\gamma \rightarrow 0$. This behavior is dictated from the forthcoming asymptotic analysis. The intuitive motivations for the first and second terms in Eq. (16) are the expressions (13) and (14). The standard upwind numerical flux is obtained by setting $\gamma = 1$, which also implies $\delta = 0$. The eventual justification for the third term $\{\mathbf{J}(\psi) \cdot \mathbf{n}\} \mathbf{\Omega}_j \cdot \mathbf{n}_1$ will come from the asymptotic analysis; this term will turn out to be necessary for the limit problem (the discretized diffusion problem derived from asymptotics) to be well-posed.

The local DG formulation of the problem Eq. (6) consists of seeking $\psi_h \in W_h$ so that the following holds for all cells $K \in \mathbb{T}_h$, for all test functions $v_j \in V_h$ supported on K , and for all direction $j \in [1, n_\Omega]$:

$$\int_K (-\psi_j \mathbf{\Omega}_j \cdot \nabla v_j + (\sigma_s + \sigma_a) \psi_j v_j - \sigma_s \bar{\psi} v_j) \, d\mathbf{x} + \int_{\partial K} \widehat{\mathbf{F}}_j(\mathbf{x}) \cdot \mathbf{n} v_j \, d\mathbf{x} = \int_K q v_j \, d\mathbf{x}. \tag{18}$$

where the numerical flux $\widehat{\mathbf{F}}_j$ is defined in (16) with γ and δ defined in (15). Eq. (18) was obtained by (i) multiplying the S_N equations for direction j with test function v_j , (ii) integrating the results by parts, and (iii) applying the numerical fluxes on the element’s boundary ∂K . With the standard expressions for $\widehat{\mathbf{F}}_j$ (recovered for $\gamma = 1$, i.e., employ the angular from within the cell on outflow faces and use the angular flux from the upwind cells on inflow faces), Eq. (18) is the standard set of equations solved element-by-element in various DG-based transport codes; see also, for instance, Eqs. (3a)–(3f) in [18] or Eq. (6) in [19].

Summing over all cells, integrating by parts a second time, and separating volume and interface terms, we obtain a global formulation which is more suitable for the asymptotic analysis. Upon introducing the bilinear form

$$\begin{aligned} \mathcal{L}(\psi, v) = & \sum_{K \in \mathbb{T}_h} \sum_{j=1}^{n_\Omega} \omega_j \int_K (\mathbf{\Omega}_j \cdot \nabla \psi_j v_j + (\sigma_s + \sigma_a) \psi_j v_j - \sigma_s \bar{\psi} v_j) \, d\mathbf{x} + \sum_{F \in F_h^b} \sum_{\mathbf{\Omega}_j \cdot \mathbf{n} \leq 0} \omega_j \int_F |\mathbf{\Omega}_j \cdot \mathbf{n}| \psi_j v_j \, d\mathbf{x} + \sum_{F \in F_h^i} \int_F \delta(\mathbf{x}) \\ & \times \{\mathbf{J}(\psi) \cdot \mathbf{n}\} \{\mathbf{J}(v) \cdot \mathbf{n}\} \, d\mathbf{x} + \sum_{F \in F_h^i} \sum_{j=1}^{n_\Omega} \omega_j \int_F \left(|\mathbf{\Omega}_j \cdot \mathbf{n}| \frac{\gamma(\mathbf{x})}{2} \llbracket \psi_j \rrbracket \llbracket v_j \rrbracket - 2\mathbf{\Omega}_j \cdot \{\{\psi_j \mathbf{n}\}\} \{v_j\} \right) \, d\mathbf{x} \end{aligned} \tag{19}$$

and the linear form

$$\ell(v) = \int_{\mathcal{D}} \sum_{j=1}^{n_\Omega} \omega_j q v_j \, d\mathbf{x} + \sum_{F \in F_h^b} \sum_{\mathbf{\Omega}_j \cdot \mathbf{n} \leq 0} \omega_j \int_F |\mathbf{\Omega}_j \cdot \mathbf{n}| \psi_j^{\text{inc}} v_j \, d\mathbf{x}, \tag{20}$$

the global version of Eq. (18) reads: seek $\psi := (\psi_1, \dots, \psi_{n_\Omega}) \in W_h$ so that the following holds:

$$\mathcal{L}(\psi, v) = \ell(v), \quad \forall v := (v_1, \dots, v_{n_\Omega}) \in W_h. \tag{21}$$

The bilinear form Eq. (19) differs from the standard upwind DG method [1,15,16] only in the choice of the parameters γ and δ . It has been pointed out in [4,7] that the upwind numerical flux is nothing more than a stabilized numerical flux, where the stabilization parameter has been arbitrarily chosen to be $\gamma = 1$ (and thus $\delta = 0$); therefore, we are not introducing a new parameter into the method, but rather we acknowledge that it has always been there in a specialized form. Also note that the proposed formulation reverts to the standard upwind form for small values of σ_s , since for $\sigma_s < \gamma_0/\text{diam}\mathcal{D}$, Eq. (15) yields $\gamma = 1$ and $\delta = 0$. Thus, the proposed method reduces the amount of upwind stabilization when the standard (upwind) stabilization is too strong.

4. Asymptotic analysis

4.1. The rescaled problem

In order to understand the behavior of solutions to Eq. (21) in the thick diffusive limit, we rescale the equation under the assumption that the ratio between the mean free path between two scattering events and the characteristic size (diameter) of the domain goes to zero. A measure of this ratio is given by

$$\varepsilon = \frac{1}{\sigma_s \text{diam}(\mathcal{D})}. \tag{22}$$

This parameter is well known to characterize the diffusivity of the problem, see for instance [12,6, Chapter XXI]. We assume throughout this section that σ_s is constant over the domain to simplify the analysis. Then, we assume the following behaviors

$$\sigma_s = \varepsilon^{-1} \tilde{\sigma}_s, \quad \sigma_a = \varepsilon \tilde{\sigma}_a, \quad q = \varepsilon \tilde{q}, \tag{23}$$

where the tilde quantities are independent of ε (note in particular that $\tilde{\sigma}_s = 1/\text{diam}(\mathcal{D})$). As ε goes to zero, the scattering and total cross sections take large values and the absorption cross section becomes small, rendering the configuration optically thick and diffusive.

Using Eq. (23), the scaled version of the transport Eq. (1) becomes

$$\boldsymbol{\Omega} \cdot \nabla \Psi(\boldsymbol{\Omega}, \mathbf{x}) + \left(\frac{\tilde{\sigma}_s}{\varepsilon} + \varepsilon \tilde{\sigma}_a \right) \Psi(\boldsymbol{\Omega}, \mathbf{x}) - \frac{\tilde{\sigma}_s}{\varepsilon} \bar{\Psi}(\mathbf{x}) = \varepsilon \tilde{q}(\mathbf{x}). \tag{24}$$

It is now well understood (see e.g., [5,12,6, Chapter XXI]) that

$$\lim_{\varepsilon \rightarrow 0} \Psi(\boldsymbol{\Omega}, \mathbf{x}) = \lim_{\varepsilon \rightarrow 0} \bar{\Psi}(\mathbf{x}) = \varphi(\mathbf{x}),$$

where the scalar flux φ satisfies the diffusion problem

$$-\nabla \cdot \left(\frac{1}{3\tilde{\sigma}_s} \nabla \varphi \right) + \tilde{\sigma}_a \varphi = \tilde{q}, \tag{25}$$

with a Dirichlet boundary condition whose exact form can be found in [5, p. 109]. We point out, that under the assumptions made for the angular quadrature, the diffusion limit of the solution to the semi-discrete problem Eq. (6) (discrete-ordinate transport equation) has the same limit properties

$$\lim_{\varepsilon \rightarrow 0} \psi_j(\mathbf{x}) = \lim_{\varepsilon \rightarrow 0} \bar{\psi}(\mathbf{x}) = \varphi(\mathbf{x}), \quad \forall j \in [1, n_\Omega].$$

The purpose of the next section is to analyze the limit of the discrete problem Eq. (21) (spatially discretized discrete-ordinate transport equation) as ε goes to zero, with the mesh size h held constant. In particular, we want to investigate whether the DG approximation Eq. (21) reduces to a consistent and convergent approximation of the diffusion equation, Eq. (25), as $\varepsilon \rightarrow 0$.

4.2. The limit problem as $\varepsilon \rightarrow 0$

Using Eq. (22) in the definition of γ and δ , see Eq. (15), and considering the limit as ε goes to zero (i.e., $\varepsilon < \gamma_0$), we obtain

$$\gamma = \gamma_0 \varepsilon, \quad \delta = \delta_0 \left(\frac{1}{\gamma_0 \varepsilon} - 1 \right). \tag{26}$$

Then, accounting for the scaling defined in Eq. (23), the scaled DG-formulation consists of seeking $\psi \in W_h$ so that the following holds for all $v \in W_h$:

$$\begin{aligned} & \sum_{K \in \mathbb{T}_h} \int_K \sum_{j=1}^{n_\Omega} \omega_j \left(\boldsymbol{\Omega}_j \cdot \nabla \psi_j v_j + \left(\frac{\tilde{\sigma}_s}{\varepsilon} + \varepsilon \tilde{\sigma}_a \right) \psi_j v_j - \frac{\tilde{\sigma}_s}{\varepsilon} \bar{\psi} v_j \right) \mathbf{d}\mathbf{x} + \sum_{F \in \mathbb{F}_h^b} \sum_{\boldsymbol{\Omega}_j \cdot \mathbf{n} \leq 0} \omega_j \int_F |\boldsymbol{\Omega}_j \cdot \mathbf{n}| \psi_j v_j \mathbf{d}\mathbf{x} + \delta_0 \left(\frac{1}{\gamma_0 \varepsilon} - 1 \right) \\ & \times \sum_{F \in \mathbb{F}_h^i} \int_F \{ \{ \mathbf{J}(\psi) \cdot \mathbf{n} \} \} \{ \{ \mathbf{J}(v) \cdot \mathbf{n} \} \} \mathbf{d}\mathbf{x} + \sum_{F \in \mathbb{F}_h^i} \int_F \sum_{j=1}^{n_\Omega} \omega_j \left(|\boldsymbol{\Omega}_j \cdot \mathbf{n}| \frac{\gamma_0 \varepsilon}{2} \llbracket \psi_j \rrbracket \llbracket v_j \rrbracket - 2 \boldsymbol{\Omega}_j \cdot \{ \{ \psi_j \mathbf{n} \} \} \{ \{ v_j \} \} \right) \mathbf{d}\mathbf{x} \\ & = \int_{\mathcal{D}} \varepsilon \tilde{q} v \mathbf{d}\mathbf{x} + \sum_{F \in \mathbb{F}_h^b} \sum_{\boldsymbol{\Omega}_j \cdot \mathbf{n} \leq 0} \omega_j \int_F |\boldsymbol{\Omega}_j \cdot \mathbf{n}| \psi_j^{\text{inc}} v_j \mathbf{d}\mathbf{x}. \end{aligned} \tag{27}$$

In the rest of the asymptotic analysis we only consider $\psi^{\text{inc}} = 0$ and we refer the reader to [8] for the handling of inhomogeneous Dirichlet boundary conditions. The main result of our asymptotic analysis is the following:

Proposition 1. *Let $\psi \in W_h$ be the solution to the scaled S_N -DG problem Eq. (27). Then, as $\varepsilon \rightarrow 0$, ψ converges to an isotropic function $\varphi \in V_{0,h}$. Furthermore, there is a vector field $\mathbf{J} \in (V_h)^d$ so that the pair (φ, \mathbf{J}) solves the following DG system for all $v \in V_{0,h}$ and all $\mathbf{L} \in (V_h)^d$:*

$$\begin{aligned} & \sum_{K \in \mathbb{T}_h} \int_K (\nabla \cdot \mathbf{J} + \tilde{\sigma}_a \varphi) v \mathbf{d}\mathbf{x} + \sum_{F \in \mathbb{F}_h^b} \int_F \left(c_{\mathbf{n}_F} \frac{\gamma_0}{2} \llbracket \varphi \rrbracket \llbracket v \rrbracket - 2 \{ \{ \mathbf{J} \cdot \mathbf{n} \} \} \{ \{ v \} \} \right) \mathbf{d}\mathbf{x} = \int_{\mathcal{D}} \tilde{q} v \mathbf{d}\mathbf{x}, \\ & \sum_{K \in \mathbb{T}_h} \int_K \left(\frac{1}{3} \nabla \varphi + \tilde{\sigma}_s \mathbf{J} \right) \cdot \mathbf{L} \mathbf{d}\mathbf{x} + \sum_{F \in \mathbb{F}_h^i} \int_F \left(-\frac{2}{3} \{ \{ \varphi \mathbf{n} \} \} \{ \{ \mathbf{L} \} \} + \frac{\delta_0}{3\gamma_0} \{ \{ \mathbf{J} \cdot \mathbf{n} \} \} \{ \{ \mathbf{L} \cdot \mathbf{n} \} \} \right) \mathbf{d}\mathbf{x} = 0, \end{aligned} \tag{28}$$

where $c_{\mathbf{n}_F} := \sum_{\boldsymbol{\Omega}_j \cdot \mathbf{n}_F \leq 0} \omega_j |\boldsymbol{\Omega}_j \cdot \mathbf{n}_F|$ is bounded away from zero uniformly with respect to $F \in \mathbb{F}_h^i, h$, and n_Ω .

The system (28) coincides exactly with the method from [7, Section 5.3] on the interior cells of the domain. The two methods differ only at the boundary, where the present method implements the zero boundary condition strongly. Since this difference in the implementation of the boundary condition is non-essential, we conclude from the theoretical convergence analysis in [7] that (28) is a consistent and convergent approximation of (25). That is, the discrete transport formulation Eq. (27) is robust and yields a convergent approximation of the diffusion equation as ε goes to zero.

We restrict ourselves to a formal asymptotic derivation. A complete rigorous convergence proof can be made by adapting the arguments from [8, Section 4] to the present case.

The formal asymptotic argument consists of assuming that the angular flux can be expanded in powers of ε as follows:

$$\psi = \psi^{(0)} + \varepsilon\psi^{(1)} + \varepsilon^2\psi^{(2)} + \mathcal{O}(\varepsilon^3).$$

Then, we insert this ansatz in Eq. (27) and separate the terms involving different powers of ε . This yields equations for the terms involving ε^{-1} , ε^0 , ε , etc.

Step 1: Terms involving ε^{-1} : isolating the terms of negative order in ε in Eq. (27) yields

$$\sum_{j=1}^{n_\Omega} \omega_j \int_D \tilde{\sigma}_s (\psi_j^{(0)} - \overline{\psi^{(0)}}) v_j \mathbf{d}\mathbf{x} + \frac{\delta_0}{\gamma_0} \sum_{F \in \mathbb{F}_h^i} \int_F \{ \{ \mathbf{J}(\psi^{(0)}) \cdot \mathbf{n} \} \} \{ \{ \mathbf{J}(v) \cdot \mathbf{n} \} \} \mathbf{d}\mathbf{x} = 0,$$

for every $v \in W_h$. Taking $v = \psi^{(0)} - \overline{\psi^{(0)}}$ in the above equality and observing that $\mathbf{J}(\overline{\psi^{(0)}}) = 0$ yields

$$\sum_{j=1}^{n_\Omega} \omega_j \int_D \tilde{\sigma}_s (\psi_j^{(0)} - \overline{\psi^{(0)}})^2 \mathbf{d}\mathbf{x} + \frac{\delta_0}{\gamma_0} \sum_{F \in \mathbb{F}_h^i} \int_F \{ \{ \mathbf{J}(\psi^{(0)}) \cdot \mathbf{n} \} \}^2 \mathbf{d}\mathbf{x} = 0.$$

Upon observing that the integrands in both terms are squared and that the sum has to be zero, we conclude that $\psi_j^{(0)} = \overline{\psi^{(0)}}$ for all $j \in [1, n_\Omega]$, i.e., the leading order of the angular flux $\psi^{(0)}$ is isotropic.

Step 2: Terms involving ε^0 : We continue the asymptotic analysis by considering the terms of the next leading order, ε^0 , which yields

$$\begin{aligned} \sum_{K \in \mathbb{T}_h} \sum_{j=1}^{n_\Omega} \omega_j \int_K (\boldsymbol{\Omega}_j \cdot \nabla \psi_j^{(0)} + \tilde{\sigma}_s (\psi_j^{(0)} - \overline{\psi^{(0)}})) v_j \mathbf{d}\mathbf{x} - \sum_{F \in \mathbb{F}_h^i} \sum_{j=1}^{n_\Omega} \omega_j \int_F 2\boldsymbol{\Omega}_j \cdot \{ \{ \psi_j^{(0)} \mathbf{n} \} \} \{ \{ v_j \} \} \mathbf{d}\mathbf{x} + \delta_0 \sum_{F \in \mathbb{F}_h^b} \int_F \{ \{ \mathbf{J}(\gamma_0^{-1} \psi^{(1)} - \psi^{(0)}) \cdot \mathbf{n} \} \} \{ \{ \mathbf{J}(v) \cdot \mathbf{n} \} \} \mathbf{d}\mathbf{x} \\ + \sum_{F \in \mathbb{F}_h^i} \sum_{\boldsymbol{\Omega}_j \cdot \mathbf{n} \leq 0} \omega_j \int_F |\boldsymbol{\Omega}_j \cdot \mathbf{n}| \psi_j^{(0)} v_j \mathbf{d}\mathbf{x} = 0, \quad \forall v \in W_h. \end{aligned} \tag{29}$$

Testing this equation with $v = \psi^{(0)}$, which is isotropic (according to the results obtained in Step 1), we observe that only the last term in Eq. (29) is non-zero. More precisely the first term in Eq. (29) is zero owing to the symmetry property of the quadrature rule (3); the second term is zero since by definition $\sum_{1 \leq j \leq n_\Omega} \omega_j \psi_j^{(1)} = \overline{\psi^{(1)}}$; the third term is zero again owing to the symmetry property (3); the fourth term is zero since $\{ \{ \mathbf{J}(v) \cdot \mathbf{n} \} \} = 0$ for v isotropic, which is again a consequence of (3). Thus, we deduce that

$$\sum_{F \in \mathbb{F}_h^b} c_{\mathbf{n}_F} \int_F |\overline{\psi^{(0)}}|^2 \mathbf{d}\mathbf{x} = 0.$$

Owing to Eq. (5), we observe that $c_{\mathbf{n}_F}$ is uniformly bounded from below by a positive constant c_0 . This fact, together with the above equation, then implies that the leading order term is zero on the domain boundary, $\psi^{(0)}|_{\partial D} = 0$, i.e., $\psi^{(0)} \in W_{0,h}$. Next, we choose a vector-valued function $\mathbf{L} \in (V_h)^d$ and we pick the test function v such that $v_j(\mathbf{x}) = \boldsymbol{\Omega}_j \cdot \mathbf{L}(\mathbf{x})$. Next, we express each term of Eq. (29). For each cell $K \in \mathbb{T}_h$ in Eq. (29), we obtain:

$$\begin{aligned} \sum_{j=1}^{n_\Omega} \omega_j \int_K (\boldsymbol{\Omega}_j \cdot \nabla \psi_j^{(0)} + \tilde{\sigma}_s (\psi_j^{(0)} - \overline{\psi^{(0)}})) \boldsymbol{\Omega}_j \cdot \mathbf{L} \mathbf{d}\mathbf{x} &= \int_K \sum_{j=1}^{n_\Omega} \omega_j ((\boldsymbol{\Omega}_j \cdot \nabla \psi_j^{(0)}) (\boldsymbol{\Omega}_j \cdot \mathbf{L}) \mathbf{d}\mathbf{x} + \tilde{\sigma}_s \psi_j^{(0)} \boldsymbol{\Omega}_j \cdot \mathbf{L}) \\ &= \int_K \left(\frac{1}{3} \nabla \psi^{(0)} + \tilde{\sigma}_s \mathbf{J}(\psi^{(0)}) \right) \cdot \mathbf{L} \mathbf{d}\mathbf{x}. \end{aligned}$$

For each interior face $F \in \mathbb{F}_h^i$, we have

$$\begin{aligned} \sum_{j=1}^{n_\Omega} \omega_j \int_F 2\boldsymbol{\Omega}_j \cdot \{ \{ \psi_j^{(0)} \mathbf{n} \} \} \{ \{ \boldsymbol{\Omega}_j \cdot \mathbf{L} \} \} \mathbf{d}\mathbf{x} - \frac{\delta_0}{\gamma_0} \int_F \{ \{ \mathbf{J}(\psi^{(1)} - \gamma_0 \psi^{(0)}) \cdot \mathbf{n} \} \} \{ \{ \mathbf{J}(v) \cdot \mathbf{n} \} \} \mathbf{d}\mathbf{x} \\ = \int_F \left(\frac{2}{3} \{ \{ \psi_j^{(0)} \mathbf{n} \} \} \{ \{ \mathbf{L} \} \} - \frac{\delta_0}{3\gamma_0} \{ \{ \mathbf{J}(\psi^{(1)}) \cdot \mathbf{n} \} \} \{ \{ \mathbf{L} \cdot \mathbf{n} \} \} \right) \mathbf{d}\mathbf{x}. \end{aligned}$$

Note that we used $\mathbf{J}(\psi^{(0)}) = 0$ and $\mathbf{J}(v) \cdot \mathbf{n} = \frac{1}{3} \mathbf{L} \cdot \mathbf{n}$. The terms on the boundary faces vanish, since we have previously established that $\psi^{(0)}$ vanishes at the boundary. Now, let us introduce the notation

$$\varphi := \psi^{(0)}, \quad \mathbf{J} := \mathbf{J}(\psi^{(1)}). \tag{30}$$

Summing up the above results and using the above change of notation Eq. (30), we infer that Eq. (29) implies that the following holds for all $\mathbf{L} \in (V_h)^d$:

$$\sum_{K \in \mathbb{T}_h} \int_K \left(\frac{1}{3} \nabla \varphi + \tilde{\sigma}_s \mathbf{J} \right) \cdot \mathbf{L} \, d\mathbf{x} + \sum_{F \in \mathbb{F}_h^i} \int_F \left(-\frac{2}{3} \{ \{ \varphi \mathbf{n} \} \} \{ \{ \mathbf{L} \} \} + \frac{\delta_0}{3\gamma_0} \{ \{ \mathbf{J} \cdot \mathbf{n} \} \} \{ \{ \mathbf{L} \cdot \mathbf{n} \} \} \right) d\mathbf{x} = 0. \tag{31}$$

This is a discrete version of Fick’s law.

Step 3: Terms involving ε^1 : Finally, the terms of first order in ε in the asymptotic expansion yield the following:

$$\begin{aligned} & \sum_{K \in \mathbb{T}_h} \int_K \sum_{j=1}^{n_\Omega} \omega_j \left(\Omega_j \cdot \nabla \psi_j^{(1)} + \tilde{\sigma}_s \left(\psi_j^{(2)} - \overline{\psi^{(2)}} \right) + \tilde{\sigma}_a \psi_j^{(0)} \right) v_j \, d\mathbf{x} \\ & + \sum_{F \in \mathbb{F}_h^i} \int_F \sum_{j=1}^{n_\Omega} \omega_j \left(\frac{\gamma_0}{2} |\Omega_j \cdot \mathbf{n}| \llbracket \psi_j^{(0)} \rrbracket \llbracket v_j \rrbracket - 2\Omega_j \cdot \{ \{ \psi_j^{(1)} \mathbf{n} \} \} \{ \{ v_j \} \} \right) d\mathbf{x} + \frac{\delta_0}{\gamma_0} \sum_{F \in \mathbb{F}_h^i} \int_F \{ \{ \mathbf{J}(\psi^{(2)} - \gamma_0 \psi^{(1)}) \cdot \mathbf{n} \} \} \{ \{ v \cdot \mathbf{n} \} \} d\mathbf{x} \\ & + \sum_{F \in \mathbb{F}_h^b} \int_F \sum_{\Omega_j \cdot \mathbf{n} \leq 0} \omega_j |\Omega_j \cdot \mathbf{n}| \psi_j^{(1)} v_j \, d\mathbf{x} = \sum_{j=1}^{n_\Omega} \omega_j \int_{\mathcal{D}} \tilde{q} v_j \, d\mathbf{x}, \quad \forall v_j \in W_h. \end{aligned} \tag{32}$$

We test Eq. (32) with an isotropic test function v with zero boundary values, i.e., $v_j = u$, for all $j \in [1, n_\Omega]$, where $u \in V_{h,0}$. We then obtain

$$\sum_{K \in \mathbb{T}_h} \int_K (\nabla \cdot \mathbf{J} + \tilde{\sigma}_a \varphi) u \, d\mathbf{x} + \sum_{F \in \mathbb{F}_h^i} \int_F \left(c_{n_f} \frac{\gamma_0}{2} \llbracket \varphi \rrbracket \llbracket u \rrbracket - 2 \{ \{ \mathbf{J} \cdot \mathbf{n} \} \} \{ \{ u \} \} \right) d\mathbf{x} = \int_{\mathcal{D}} \tilde{q} u \, d\mathbf{x}. \tag{33}$$

This is a discrete balance equation. Equations Eqs. (33) and (31) are a DG discretization of the diffusion equation Eq. (25) written in mixed form. This completes the derivation of our main asymptotic result.

5. One-dimensional numerical experiments

In this section, we compare the reduced-upwind method proposed in this paper with the standard upwind method for typical one-dimensional radiation transport test problems published in the literature. Note that the standard solution technique based on transport sweeps may not be applicable anymore, because downwind angular information is required in the proposed method. Efficient preconditioning methods are currently being developed for the proposed method, and our findings will be reported in a future communication. Since the numerical experiments presented in this section deal exclusively with one-dimensional problems, the discrete S_N equations are solved by direct inversion of the entire linear system.

Since the linear discontinuous finite element (DG1) discretization with standard upwinding does not lock in the thick diffusive limit in one space dimension, we mostly present results obtained using the constant discontinuous (DG0) spatial discretization. Most of the numerical tests shown have been proposed in Larsen et al. [12]. All the calculations are performed using the S_8 Gauss–Legendre quadrature. We used $\gamma_0 = 2$ and $\delta_0 = 1$ in all the calculations. In agreement with the above asymptotic analysis, numerical tests, not reported here, have shown that the method performs well and does not depend much on γ_0 and δ_0 provided these two coefficients are of order one. All the numerical results are compared with the analytical S_8 solutions which have been obtained using the Maple scripts of [17].

The units employed to measure lengths are denoted *unitL*; the units for the scalar flux, angular flux, and volumetric source are denoted *unitΦ*, *unitΨ*, and *unitS*, respectively. For instance, it is usual in the literature to take *unitL* to be cm and *unitΦ* to be particles/cm²/s.

5.1. Problem A

The first test case that we consider is problem #1 from [12]. A constant volumetric source is placed in a highly diffusive, pure scatterer ($\sigma_a = 0$, $\sigma_s = 100 \text{ unitL}^{-1}$, domain length of 10 unitL , $q = 0.01 \text{ unitS}$) with vacuum boundary conditions.

We show in Fig. 1 the scalar flux computed using DG0 on four meshes composed of 10, 20, 40, and 500 cells, respectively. For each mesh we compare the solution obtained with the new reduced upwind method, the solution obtained with standard upwinding and the S_8 analytical solution. The solution with standard upwinding locks even with 500 cells. This test demonstrates well that the reduced upwind method is better than standard upwinding for highly diffusive configurations. For instance, the new method provides vastly superior results than the standard one on coarse cells (10 cells total, each 100 mfp thick). The new method converges significantly faster than the standard one to the exact analytical solution when the mesh is refined.

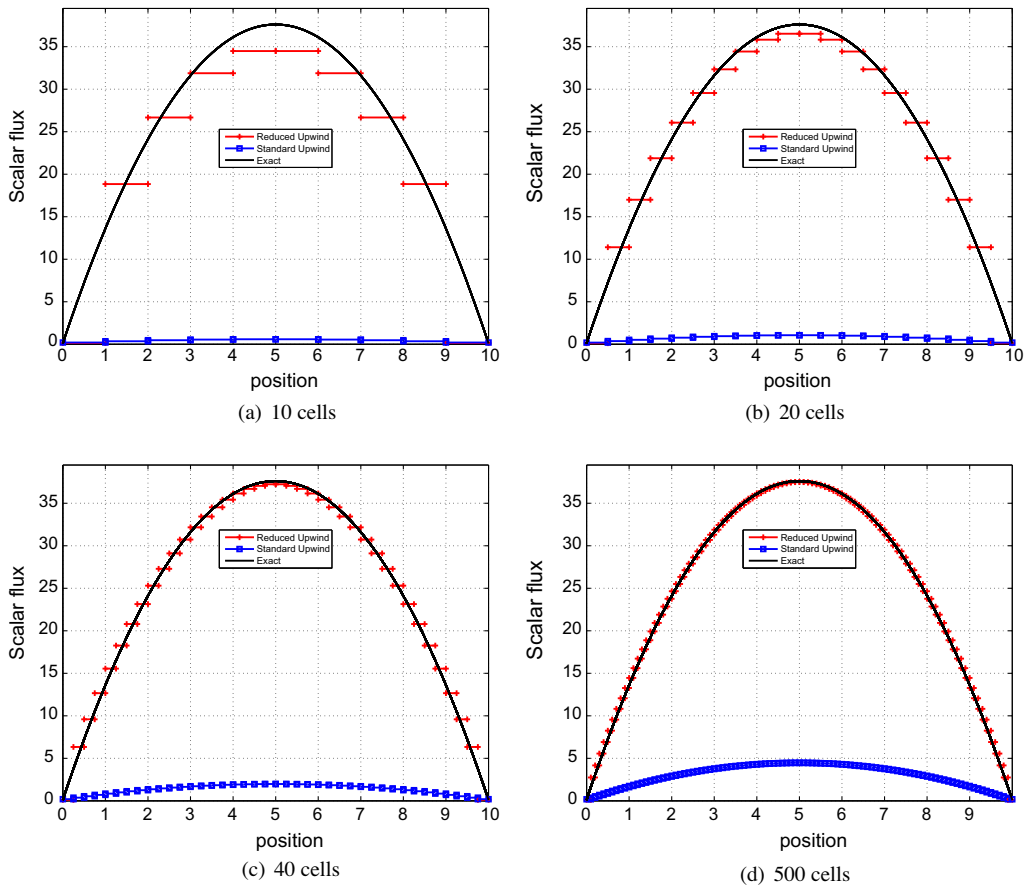


Fig. 1. DG0 Scalar flux solutions for Problem A with various mesh resolutions.

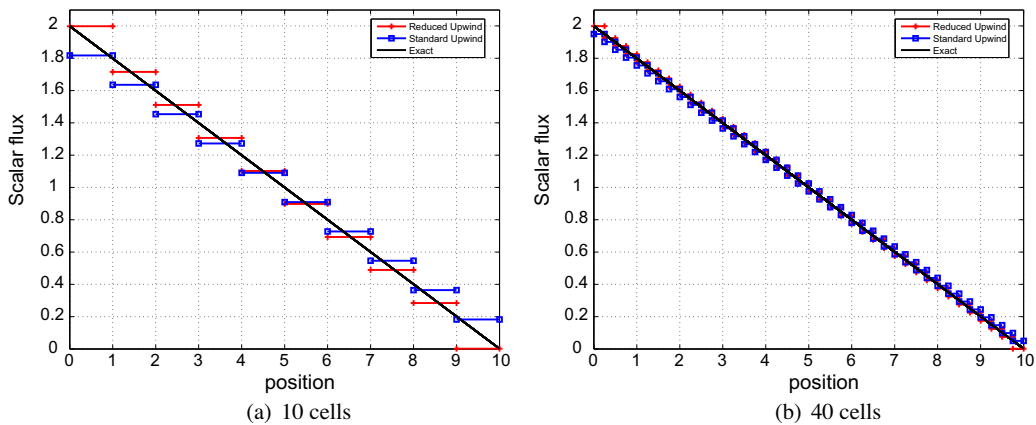


Fig. 2. DG0 Scalar flux solutions for Problem B with various mesh resolutions.

5.2. Problem B

The second test case that we consider is problem #2 from [12]. An isotropic unit boundary source, placed at $x = 0$, radiates onto a highly diffusive pure scatterer ($\sigma_a = 0$, $\sigma_s = 100 \text{ unitL}^{-1}$, domain length of 10 unitL). Fig. 2 shows that for DG0, the standard upwind and the reduced upwind methods both give reasonable approximations of the exact solution. No locking is observed in this test case.

5.3. Problem C

The third test case that we consider is problem #4 from [12]. A quasi-normally incident beam radiates from the left onto a highly diffusive pure scatterer ($\sigma_a = 0$, $\sigma_s = 100 \text{ unitL}^{-1}$, domain length of 10 unitL). The incident angular flux is $\frac{1}{\omega_N} \text{ unit}\Psi$, where ω_N is the quadrature weight associated with the direction closest to the normal in the S_N Gauss–Legendre quadrature set. This pencil beam problem develops a narrow boundary layer at $x = 0$.

The results shown in Fig. 3 indicate again that the reduced upwind method performs better than standard upwinding for the DG0 approximation. For instance, one observes in the right panel of Fig. 3 that the DG0 discretization with reduced upwinding attempts at capturing the boundary layer effect whereas the standard upwind technique seems to ignore it completely.

In [12], a variation of this problem (labeled problem #5 in [12]) employs a fine mesh in which the first 0.05 unitL of the domain is discretized using 50 cells and the remainder of the domain is discretized using 10 cells; thus, a total of 60 cells is used. We show the corresponding DG0 results in Fig. 4. The benefits of the new method are obvious.

We show in Fig. 5 the solution to the above problem using the DG1 approximation with 10 and 40 cells. The reduced and the standard upwind methods perform equally well. After the first cell, both approximations are indistinguishable and the two curves coincide. This is not a surprise since it is known that DG1 does not lock in one space dimension with the standard upwind method. It seems that the scalar flux of the DG1 approximation with reduced upwinding slightly overshoots in the boundary layer; however, the reduced upwind method yields an average scalar flux in the first cell that is more accurate than the one resulting from the standard upwind method. Simulations run on the refined mesh defined above with the DG1 approximation reveal that both techniques give very similar results. We do not show these results here for conciseness.

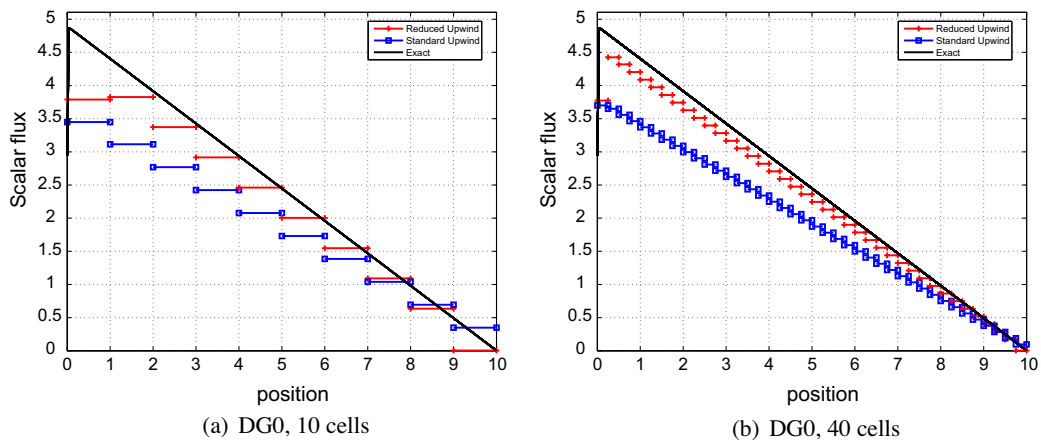


Fig. 3. DG0 Scalar flux solutions for Problem C.

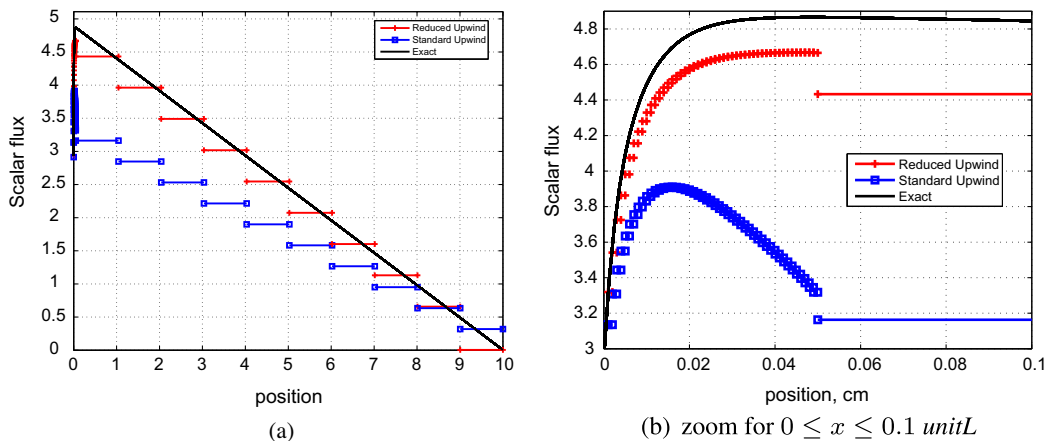


Fig. 4. DG0 scalar flux solutions for Problem C, fine discretization in the boundary layer.

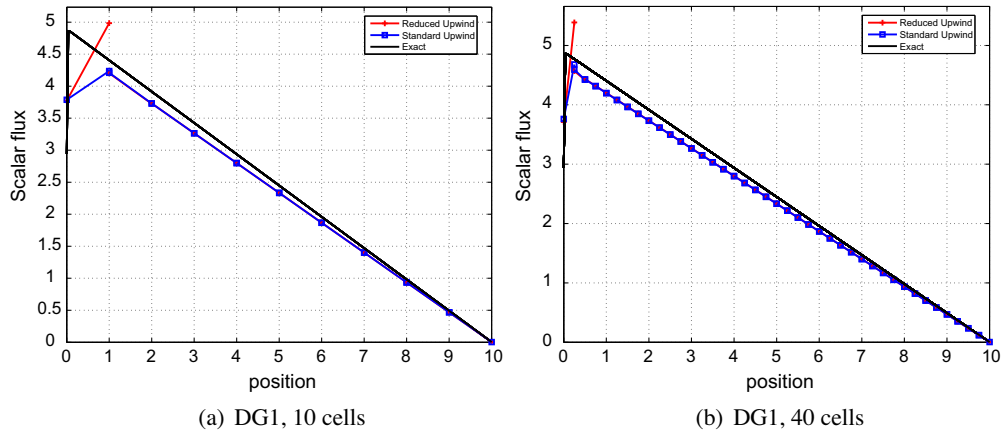


Fig. 5. DG1 Scalar flux solutions for Problem C.

5.4. Problem D

In this fourth test case we solve the transport equation in a domain of length 1 *unitL* and the total and scattering cross sections are: $\sigma_t = \frac{1}{\epsilon} \text{ unitL}^{-1}$ and $\sigma_s = (\frac{1}{\epsilon} - \epsilon) \text{ unitL}^{-1}$, respectively. The parameter ϵ takes the following values: 10^{-2} , 10^{-3} , 10^{-4} . As ϵ decreases the problem configuration is increasingly optically thick and diffusive: σ_t values are 10^2 , 10^3 , 10^4 unitL^{-1} , respectively. The associated scattering ratio, $c = \frac{\sigma_s}{\sigma_t}$, are 0.9999, 0.999999, and 0.99999999, respectively. Vacuum boundary conditions apply and a unit volumetric source is used.

We show in Fig. 6 the numerical solutions obtained with the new technique (left panel) and the standard upwind technique (right panel) for the various predefined values of ϵ . The analytical solutions are also shown in each case. Again, it is clear that the new technique is vastly superior to the standard upwinding. We note that as $\epsilon \rightarrow 0$, the standard upwind technique locks, i.e., it yields the continuous zero solution (a well-known result), whereas the new technique does not show this flaw.

We show in Fig. 7 the solutions obtained with $\epsilon = 10^{-4}$ and various mesh resolutions (10, 20, and 40 mesh cells). The new technique converges towards the analytical solution as the mesh is refined, even for very thick and diffusive material configurations, whereas the solution obtained with the standard upwind method locks and tends toward the zero solution.

5.5. Problem E

In the last test case we consider a domain composed of two different materials. Three different configurations are considered. In material region 1 ($0 < x < 0.5 \text{ unitL}$), $\sigma_{s,1}$ is held constant and set to 100 unitL^{-1} . In the material in region 2

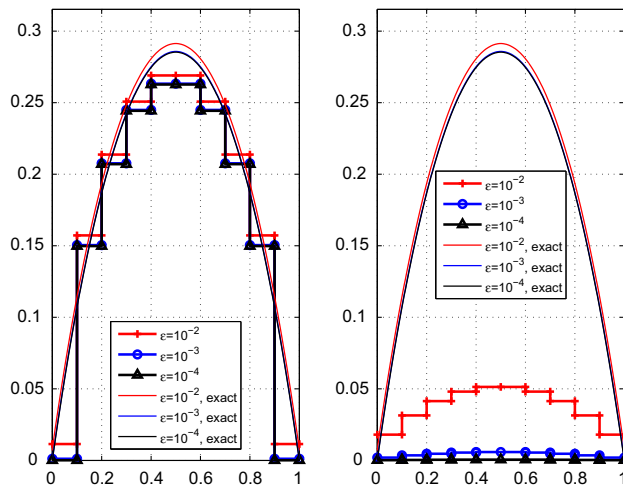


Fig. 6. DG0 scalar flux solutions for Problem D for $\epsilon = 10^{-2}$, 10^{-3} , and 10^{-4} (left panel: reduced upwind scheme and exact solutions; right panel: standard upwind scheme and exact solutions).

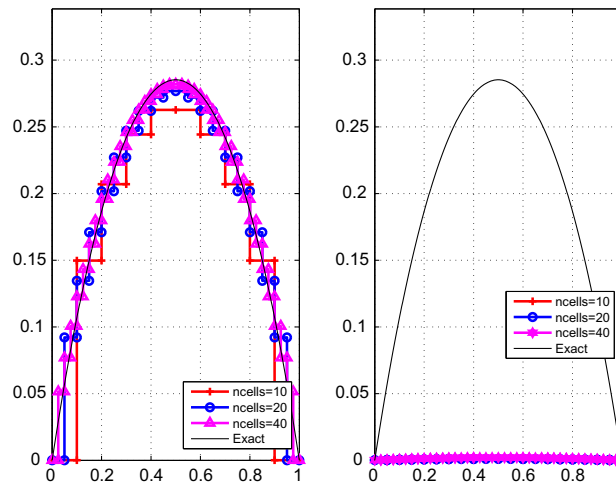


Fig. 7. DG0 scalar flux solutions for Problem D with $\varepsilon = 10^{-4}$ and various mesh refinements (left panel: reduced upwind scheme and exact solutions; right panel: standard upwind scheme and exact solutions).

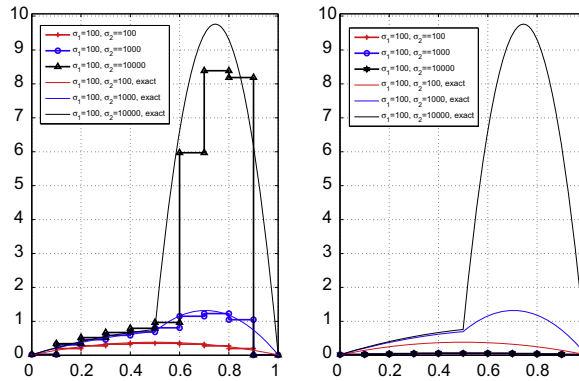


Fig. 8. DG0 scalar flux solutions for Problem E with 10 spatial cells: new upwind formulation (left panel), standard upwind formulation (right panel).

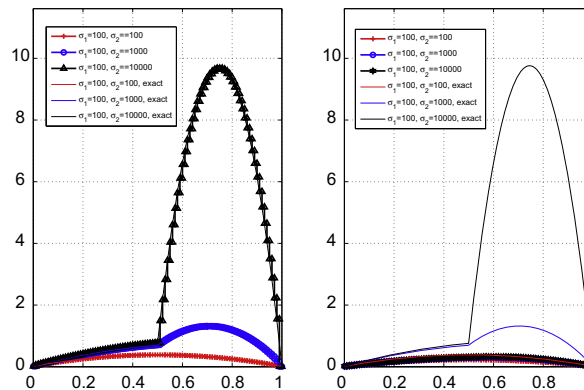


Fig. 9. DG0 scalar flux solutions for Problem E with 100 spatial cells: new upwind formulation (left panel), standard upwind formulation (right panel).

($0.5 < x < 1 \text{ unitL}$) $\sigma_{s,2}$ is uniformly constant and is either 10^2 , 10^3 , or 10^4 unitL^{-1} . Both materials in region 1 and region 2 are pure scatterers (i.e., $\sigma_a = 0$). The problem configuration is progressively made more and more heterogeneous as $\sigma_{s,2}$ increases. The domain's optical thicknesses for these three tests are 100, 550, and 5050 mean free paths, respectively. In both regions, a constant isotropic volumetric source of strength 10^{-2} unitS is used. The configuration is placed in vacuum.

We show in Fig. 8 the results obtained with DG0 on a mesh composed of 10 cells uniformly distributed. The left panel shows the results obtained with the reduced upwinding and the right panel shows the results obtained with the standard upwind method. We observe, again, that the standard method locks whereas the new method performs very well considering the small number of cells used.

We show in Fig. 9 the results obtained with DG0 on a mesh composed of 100 cells uniformly distributed. Again, the reduced upwind method performs very well. The standard method locks on this fine mesh when $\sigma_{s,2}$ equal to 10^3 and 10^4 unitL^{-1} .

6. Conclusions

A new, unconditionally stable, discontinuous Galerkin method for radiative transfer and neutron transport problems has been introduced. The scheme is based on a reduced upwind stabilization, as opposed to the standard upwinding commonly used in particle transport problems. This new scheme has been tested with standard one-dimensional (slab) test cases and has been found to perform well in all regimes, from transport-dominated to diffusion-dominated situations, and for piecewise constant (DG0) and piecewise linear (DG1) approximations. In this respect, the piecewise constant version of the new method performs significantly better than the classical finite-volume “step” scheme. Depending on the relative magnitude of the scattering cross section, the new numerical flux is defined so that the method reverts back to the standard upwind technique in transport-dominated regimes.

From the point of view of implementation, a current drawback of the new scheme is that the resulting transport operator for a given direction cannot be inverted exactly with a transport sweep anymore, since downwind angular flux contributions may have to be accounted for. We conjecture, but have not thoroughly investigated the issue yet, that inexact sweeps, as applied in [9] are a good substitute, in particular when used in conjunction with diffusion acceleration techniques. This is motivated by the observation that (i) our method reverts to standard upwind in the scattering-free case, and (ii) transport sweep solutions decay very fast in diffusion-dominated regimes. We are planning to apply a multigrid technique directly to the radiation operator and devise a robust smoother. Furthermore, performing multi-dimensional tests to assess the accuracy and effectiveness of this method are also planned, and will be subsequently communicated, along with a rigorous mathematical convergence analysis of the new scheme.

Appendix A. DG formulations for 1D slab problems

We derive in this Appendix explicit formulas for the weak formulations in one-dimensional slab geometries, $[0, L]$. Specifically, we provide expressions for the piece-wise constant (DG0) and linear discontinuous (DG1) approximations with vacuum boundary conditions, isotropic scattering, and isotropic external source. The S_N approximation of this problem can be formulated as follows:

$$\mu_j \frac{d\psi_j}{dx} + \sigma_t \psi_j = \sigma_s \bar{\psi} + q, \quad \text{for } j \in [1, n_\Omega], \tag{A.1}$$

$$\bar{\psi} = \sum_{j=1}^{n_\Omega} \omega_j \psi_j, \tag{A.2}$$

where the angular cosines μ_j are the x -components of the quadrature directions Ω_j . The array $(\psi_1, \dots, \psi_{n_\Omega})$ is the vector of angular fluxes and $\bar{\psi}$ is the scalar flux. We use standard notation from finite volume methods to recast the weak formulation. The slab is split into N elements, resulting in the following spatial grid: $0 = x_{1/2} < x_{3/2} < \dots < x_{i-1/2} < x_{i+1/2} < \dots < x_{N+1/2} = L$ with local mesh size $\Delta_i = x_{i+1/2} - x_{i-1/2}$. We assume that the material properties and the external source are piece-wise constant, and we denote these quantities with $\sigma_{t,i} = \sigma_t|_{[x_{i-1/2}, x_{i+1/2}]}$ and $q_i = q|_{[x_{i-1/2}, x_{i+1/2}]}$.

Starting from Eq. (18), we write the local DG bilinear form for a single element $K_i = [x_{i-1/2}, x_{i+1/2}]$ and for a given angular direction $j \in [1, n_\Omega]$ as follows:

$$\begin{aligned} & \int_{x_{i-1/2}}^{x_{i+1/2}} \left(-\mu_j \psi_j(x) \frac{dv_j^i}{dx} + \sigma_{t,i} \psi_j(x) v_j^i(x) \right) dx - \widehat{F}_j^-(x_{i-1/2}) v_j^i(x_{i-1/2}) + \widehat{F}_j^+(x_{i+1/2}) v_j^i(x_{i+1/2}) \\ & = \sigma_{s,i} \int_{x_{i-1/2}}^{x_{i+1/2}} \bar{\psi}(x) v_j^i(x) dx + q_i \int_{x_{i-1/2}}^{x_{i+1/2}} v_j^i(x) dx, \end{aligned} \tag{A.3}$$

where v_j^i is any test function for direction μ_j supported in the element K_i . In order to define the numerical flux \widehat{F}_j^\pm , let us denote by $\psi_j^i(x)$ the restriction of the angular flux in direction μ_j to the interval K_i , and $J^i(x) = \sum_{j=1}^{n_\Omega} \omega_j \mu_j \psi_j^i(x)$ accordingly. Then, taking into account that “normal vectors” are either +1 or -1, the one-dimensional version of (16) becomes

$$\pm \widehat{F}_j^\pm(x_{i+1/2}) = \pm \mu_j \frac{\psi_j^i(x_{i+1/2}) + \psi_j^{i+1}(x_{i+1/2})}{2} \pm \frac{\gamma_{i+1/2}}{2} |\mu_j| \left(\psi_j^i(x_{i+1/2}) - \psi_j^{i+1}(x_{i+1/2}) \right) \pm \frac{\delta_{i+1/2}}{2} \mu_j \frac{J^i(x_{i+1/2}) - J^{i+1}(x_{i+1/2})}{2} \tag{A.4}$$

Here, the superscripts “+” and “-” refer to the positive and negative sign of the normal of the interval at $x_{i+1/2}$, respectively.

When $\gamma = 1$ (and thus $\delta = 0$), the expressions for the numerical fluxes at $x_{i-1/2}$ and $x_{i+1/2}$ simplify to the standard upwind values:

$$\widehat{F}_j^\pm(x_{i+1/2}) = \widehat{F}_j^\pm(x_{i+1/2}) = \begin{cases} \mu_j \psi_j^i(x_{i+1/2}) & \text{if } \mu_j \geq 0, \\ \mu_j \psi_j^{i+1}(x_{i+1/2}) & \text{if } \mu_j < 0. \end{cases} \tag{A.5}$$

A.1. Expressions for DGO

In the DGO setting the approximation is piece-wise constant, and there is only one scalar shape function per element.

$$v^i(x) = \begin{cases} 1 & \text{if } x \in K = [x_{i-1/2}, x_{i+1/2}], \\ 0 & \text{otherwise,} \end{cases} \tag{A.6}$$

and there is only one unknown per element per angular direction j , i.e., $\psi_j(x) = \sum_{i=1}^N \psi_j^i v^i(x)$. This implies that $\psi_j(x) = \psi_j^i$ in the element $K_i = [x_{i-1/2}, x_{i+1/2}]$. Furthermore, the vector flux is constant and we let $J^i = J^i(x)$ on K_i with the convention that $J^0 = 0$ and $J^{N+1} = 0$. Inserting these definitions into (A.4), we obtain

$$\pm \widehat{F}_j^\pm(x_{i+1/2}) = \pm \mu_j \frac{\psi_j^i + \psi_j^{i+1}}{2} \pm \frac{\gamma_{i+1/2}}{2} |\mu_j| (\psi_j^i - \psi_j^{i+1}) \pm \frac{\delta_{i+1/2}}{2} \mu_j \frac{J^i - J^{i+1}}{2}. \tag{A.7}$$

In combination with (A.3), we infer that the set of coupled equations to be solved for the $N \times n_\Omega$ unknowns $\{\psi_j^i\}_{1 \leq i \leq N, 1 \leq j \leq n_\Omega}$ is

$$\begin{aligned} & \left(\sigma_{t,i} \Delta_i + \frac{\gamma_{i-1/2} + \gamma_{i+1/2}}{2} |\mu_j| \right) \psi_j^i + \frac{\mu_j - \gamma_{i+1/2} |\mu_j|}{2} \psi_j^{i+1} - \frac{\mu_j + \gamma_{i-1/2} |\mu_j|}{2} \psi_j^{i-1} \\ & = \sigma_{s,i} \bar{\psi}_i \Delta_i + q_i \Delta_i + \frac{\mu_j}{4} \left(\delta_{i+1/2} J^{i+1} - (\delta_{i-1/2} + \delta_{i+1/2}) J^i + \delta_{i-1/2} J^{i-1} \right). \end{aligned} \tag{A.8}$$

Next, we reproduce the arguments of the asymptotic derivation and specialize them to one-dimensional slab problems. We also assume that σ_s and σ_t are constant (homogeneous domain) to simplify the analysis. Using (22)–(26) and inserting the expansion $\psi_j^i = \psi_{j,0}^i + \varepsilon \psi_{j,1}^i + \varepsilon^2 \psi_{j,2}^i + \mathcal{O}(\varepsilon^3)$ into (A.8) we obtain that the following holds at the ε^{-1} order

$$\tilde{\sigma}_s \Delta_i (\psi_{j,0}^i - \bar{\psi}_0^i) - \frac{\mu_j}{4} \frac{\delta_0}{\gamma_0} (J_0^{i+1} - J_0^i) + (J_0^{i-1} - J_0^i) = 0.$$

where $J_0 = J(\psi_0)$. Multiplying this equation by $\omega_j (\psi_{j,0}^i - \bar{\psi}_0^i)$ and summing over i and j we obtain that

$$\sum_{i=1}^N \sum_{j=1}^{n_\Omega} \tilde{\sigma}_s \omega_j \Delta_i (\psi_{j,0}^i - \bar{\psi}_0^i)^2 + \frac{1}{4} \frac{\delta_0}{\gamma_0} \sum_{i=1}^{N-1} \sum_{j=1}^{n_\Omega} (J_0^{i+1} - J_0^i)^2 = 0,$$

which immediately implies that ψ_0 is isotropic and $J_0 = 0$. At the order ε^0 we obtain

$$\tilde{\sigma}_s \Delta_i (\psi_{j,1}^i - \bar{\psi}_1^i) + \frac{\mu_j}{2} (\psi_0^{i+1} - \psi_0^{i-1}) - \frac{\mu_j}{4} \frac{\delta_0}{\gamma_0} (J_1^{i+1} - 2J_1^i + J_1^{i-1}) = 0.$$

After multiplying by $\omega_j \mu_j$ and summing over j we infer, using (4), that

$$\tilde{\sigma}_s J_1^i + \frac{\psi_0^{i+1} - \psi_0^{i-1}}{6\Delta_i} - \frac{1}{12} \frac{\delta_0}{\gamma_0} \Delta_i \frac{J_1^{i+1} - 2J_1^i + J_1^{i-1}}{\Delta_i^2} = 0. \tag{A.9}$$

At the order ε we have

$$(\tilde{\sigma}_a \Delta_i + \gamma_0 |\mu_j|) \psi_0^i + \tilde{\sigma}_s (\psi_{j,2}^i - \bar{\psi}_{j,2}^i) + \frac{\mu_j}{2} (\psi_{j,1}^{i+1} - \psi_{j,1}^{i-1}) - \gamma_0 \frac{\mu_j}{2} (\psi_0^{i+1} - \psi_0^{i-1}) - \frac{\mu_j}{4} \frac{\delta_0}{\gamma_0} (J_2^{i+1} - 2J_2^i + J_2^{i-1}) - \frac{\mu_j}{4} \frac{\delta_0}{\gamma_0} (J_2^{i+1} - 2J_2^i + J_2^{i-1}) = \tilde{q} \Delta_i. \tag{A.10}$$

We multiply this equation by ω_j and sum over j to obtain that

$$\tilde{\sigma}_a \psi_0^i + \frac{J_1^{i+1} - J_1^{i-1}}{2\Delta_i} - \gamma_0 \frac{c_0}{2} \Delta_i \frac{\psi_0^{i+1} - 2\psi_0^i + \psi_0^{i-1}}{\Delta_i^2} = \tilde{q}, \tag{A.11}$$

where c_0 is the constant in (5), which in the one-dimensional case can be computed from the angular quadrature rule.

To conclude we observe now that the system (A.9)–(A.11) is a second-order (assuming the mesh is uniform) approximation of

$$\tilde{\sigma}_s J + \frac{1}{3} \partial_x \psi - \frac{1}{12} \frac{\delta_0}{\gamma_0} \Delta_i \partial_{xx} J = 0, \tag{A.12}$$

$$\tilde{\sigma}_a \psi + \partial_x J - \gamma_0 \frac{c_0}{2} \Delta_i \partial_{xx} \psi = \tilde{q}, \tag{A.13}$$

which is itself a first-order perturbation of the diffusion limit equation in mixed form. In other words, (A.9)–(A.11) is a stable first-order approximation of the diffusion limit equation as stated in our main asymptotic result. One can finally convince oneself that (A.9)–(A.11) is a stable (therefore convergent) approximation by observing that the following a priori stability estimate holds

$$\sum_{i=1}^N \tilde{\sigma}_s (J_1^i)^2 + \tilde{\sigma}_a (\psi_0^i)^2 + \frac{1}{12} \frac{\delta_0}{\gamma_0} \sum_{i=1}^{N-1} \left(\frac{J_1^{i+1} - J_1^i}{\Delta_i} \right)^2 + \gamma_0 \frac{c_0}{2} \sum_{i=1}^{N-1} \left(\frac{\psi_0^{i+1} - \psi_0^i}{\Delta_i} \right)^2 = \sum_{i=1}^N \tilde{q} \psi_0^i. \tag{A.14}$$

This estimate is obtained by multiplying (A.9) by J_1^i , multiplying (A.11) by ψ_0^i , adding the two equations, and summing over i (using the zero boundary condition).

A.2. Expressions for DG1

We now specialize Eq. (18) to the DG1 setting in one space dimension. In the DG1 setting the approximation is piece-wise linear and discontinuous. We use the following two shape functions in each element $K_i = [x_{i-1/2}, x_{i+1/2}]$:

$$v^{j,L}(x) = \begin{cases} \frac{x_{i+1/2} - x}{\Delta_i} & \text{if } x \in K_i, \\ 0 & \text{otherwise,} \end{cases} \tag{A.15}$$

$$v^{j,R}(x) = \begin{cases} \frac{x - x_{i-1/2}}{\Delta_i} & \text{if } x \in K_i, \\ 0 & \text{otherwise,} \end{cases} \tag{A.16}$$

and the angular flux in direction j is approximated as follows in the interval K_i :

$$\psi_j(x) = \psi_j^{i,L} v_j^{i,L}(x) + \psi_j^{i,R} v_j^{i,R}(x), \tag{A.17}$$

giving the following global representation: $\psi_j(x) = \sum_{i=1}^N (\psi_j^{i,L} v_j^{i,L}(x) + \psi_j^{i,R} v_j^{i,R}(x))$. Evaluating Eq. (18) with the test function $v_j^{i,L}(x)$ first and then with the test function $v_j^{i,R}(x)$ yields the following two sets of equations:

$$\frac{\mu_j}{2} (\psi_j^{i,L} + \psi_j^{i,R}) + \frac{\sigma_{t,i+1/2} \Delta_i}{6} (2\psi_j^{i,L} + \psi_j^{i,R}) = \frac{\sigma_{s,i+1/2} \Delta_i}{6} (2\overline{\psi_j^{i,L}} + \overline{\psi_j^{i,R}}) + \frac{q_{i+1/2} \Delta_i}{2} - \widehat{F}_j(x_{i-1/2}), \tag{A.18}$$

and

$$-\frac{\mu_j}{2} (\psi_j^{i,L} + \psi_j^{i,R}) + \frac{\sigma_{t,i+1/2} \Delta_i}{6} (\psi_j^{i,L} + 2\psi_j^{i,R}) = \frac{\sigma_{s,i+1/2} \Delta_i}{6} (\overline{\psi_j^{i,L}} + 2\overline{\psi_j^{i,R}}) + \frac{q_{i+1/2} \Delta_i}{2} + \widehat{F}_j(x_{i+1/2}), \tag{A.19}$$

where the expressions for the numerical fluxes are:

$$\widehat{F}_j(x_{i+1/2}) = \mu_j \frac{\psi_j^{i,R} + \psi_j^{i+1,L}}{2} + \frac{\gamma_{i+1}}{2} |\mu_j| (\psi_j^{i,R} - \psi_j^{i+1,L}) + \frac{\delta_{i+1}}{4} \mu_j (J^{i,R} - J^{i+1,L}), \tag{A.20}$$

and

$$-\widehat{F}_j(x_{i-1/2}) = -\mu_j \frac{\psi_j^{i,L} + \psi_j^{i-1,R}}{2} + \frac{\gamma_i}{2} |\mu_j| (\psi_j^{i,L} - \psi_j^{i-1,R}) - \frac{\delta_i}{4} \mu_j (J^{i,L} - J^{i-1,R}), \tag{A.21}$$

with $J^{i,L} = \sum_{j=1}^{n_\Omega} \omega_j \mu_j \psi_j^{i,L}$ and $J^{i,R} = \sum_{j=1}^{n_\Omega} \omega_j \mu_j \psi_j^{i,R}$. The set of coupled equations to be solved for the $2 \times N \times n_\Omega$ unknowns $\{\psi_j^{i,L}, \psi_j^{i,R}\}_{1 \leq i \leq N, 1 \leq j \leq n_\Omega}$ are (A.18) and (A.19). It is now a straightforward task to reproduce again the arguments the main asymptotic result. We leave the details to the reader.

References

- [1] M.L. Adams, Discontinuous finite element transport solutions in thick diffusive problems, Nucl. Sci. Eng. 137 (3) (2001) 298–333.
- [2] B. Ayuso, L.D. Marini, Discontinuous Galerkin methods for advection–diffusion–reaction problems, SIAM J. Numer. Anal. 47 (2) (2009) 1391–1420.
- [3] Ivo Babuška, Manil Suri, On locking and robustness in the finite element method, SIAM J. Numer. Anal. 29 (5) (1992) 1261–1293.
- [4] F. Brezzi, L.D. Marini, E. Süli, Discontinuous Galerkin methods for first-order hyperbolic problems, Math. Models Methods Appl. Sci. 14 (12) (2004) 1893–1903.
- [5] S. Chandrasekhar, Radiative Transfer, Oxford University Press, 1950.
- [6] R. Dautray, J.-L. Lions, Mathematical Analysis and Numerical Methods for Science and Technology, Vol. 6, Springer, 2000.
- [7] A. Ern, J.-L. Guermond, Discontinuous Galerkin methods for Friedrichs’ systems. I. General theory, SIAM J. Numer. Anal. 44 (2) (2006) 753–778.

- [8] J.-L. Guermond, G. Kanschat, Asymptotic analysis of upwind DG approximation of the radiative transport equation in the diffusive limit, *SIAM J. Numer. Anal.* 48 (1) (2010) 53–78.
- [9] G. Kanschat, Parallel and Adaptive Galerkin Methods for Radiative Transfer Problems. Dissertation, Universität Heidelberg, 1996.
- [10] E.W. Larsen, Progress Report, LA-9533-PR (September 1982) (private communication 2009), 1982.
- [11] E.W. Larsen, On numerical solutions of transport problems in the diffusion limit, *Nucl. Sci. Eng.* 83 (1983) 90–99.
- [12] E.W. Larsen, J.E. Morel, W.F. Miller Jr., Asymptotic solutions of numerical transport problems in optically thick, diffusive regimes, *J. Comput. Phys.* 69 (2) (1987) 283–324.
- [13] E.W. Larsen, J.E. Morel, Asymptotic solutions of numerical transport problems in optically thick, diffusive regimes. II, *J. Comput. Phys.* 83 (1) (1989) 212–236.
- [14] P. LeSaint, P.-A. Raviart, On a Finite Element Method for Solving the Neutron Transport Equation, in: C. de Boor (Ed.), *Mathematical Aspects of Finite Elements in Partial Differential Equations*, Academic Press, New York, 1974, pp. 89–123.
- [15] J. Pitkäranta, Discontinuous variational approximations of neutron diffusion and transport theory, *Transport Theory Statist. Phys.* 6 (4) (1977) 169–199.
- [16] W. Reed, T. Hill, Triangular mesh methods for the neutron transport equation. Tech. Rep. LA-UR-73-479, Los Alamos Scientific Laboratory, Los Alamos, NM, 1973.
- [17] J.S. Warsa, Analytical S_N solutions in heterogeneous slabs using symbolic algebra computer programs, *Ann. Nucl. Energ.* 29 (7) (2002) 851–874.
- [18] J.S. Warsa, T.A. Wareing, J.E. Morel, Krylov iterative methods and the degraded effectiveness of diffusion synthetic acceleration for multidimensional S_N calculations in problems with material discontinuities, *Nucl. Sci. Eng.* 147 (2004) 218–248.
- [19] Y. Wang, J.C. Ragusa, High-order discontinuous Galerkin method of the S_N transport equations on unstructured triangular meshes, *Ann. Nucl. Energ.* 36 (2009) 931–939.